Physical configuration and performance modeling of all-dielectric metamaterials

Akram Ahmadi and Hossein Mosallaei*
Applied Electromagnetics Lab., ECE Department, Northeastern University, Boston, Massachusetts 02115, USA
(Received 17 April 2007; revised manuscript received 20 September 2007; published 4 January 2008)

In this paper, physical concept and performance analysis of all-dielectric metamaterials are presented. Metamaterials with desired material parameters $(\pm\varepsilon, \pm\mu)$ are developed by creating electric and magnetic resonant modes. Dielectric disk and spherical particle resonators are considered as the great candidates for establishing the dipole moments (metamaterial alphabet). A full wave finite difference time domain technique is applied to comprehensively obtain the physical insights of dielectric resonators. Near-field patterns are plotted to illustrate the development of electric and magnetic dipole fields. Geometric-polarization control of the dipole moments allows ε and μ to be tailored to the application of interest. All-dielectric double negative metamaterials are designed. Engineering concerns, such as loss reduction and bandwidth enhancement are investigated.

DOI: 10.1103/PhysRevB.77.045104 PACS number(s): 42.70.Qs, 94.20.ws

I. INTRODUCTION

Metamaterials are receiving increasing attention in the scientific community in recent years due to their exciting physical properties and novel potential applications.[1–5] To achieve a metamaterial with a desired figure of merit, it is required to first create appropriate electric and magnetic dipole moments (in small-size scales) utilizing available materials and then tailor their arrangement to the application of interest. Basically, the electric and magnetic dipole moments can be envisioned as the alphabet for making metamaterials. For instance, to achieve an artificial magnetism, the most conventional approach is to implement metallic loops offering magnetic dipole moments.[6] Conductor rods can be used for producing electric dipole moments.[7] Arrangements of these dipole moments can establish required material parameters, for instance, a double negative (DNG) metamaterial behavior as depicted in Fig. 1.

Most of the metamaterial designs are constructed with the use of metallic elements. The major drawbacks in using metallic inclusions are their conduction loss and fabrication difficulties, especially in the optical frequencies. In addition, they show very narrow bandwidth resonant modes. Further, most of the known realizations are highly anisotropic composites. Recently, a new paradigm for metamaterial development was introduced by Holloway *et al.* in Ref. 8, where they used magnetodielectric spheres for generating required magnetic and electric dipole moments. Later on, Vendik *et al.* used the same concept and suggested a more practical approach, such that only dielectric spheres are involved.[9] Basically, they proposed two sets of spheres having the same dielectric materials but different radii. The dielectric material of spheres is much larger than the host material, such that the wavelength inside the spheres is comparable to their diameters, and at the same time the wavelength outside the spheres is large in comparison to the spheres sizes. The electromagnetic fields inside this composite can be viewed as the superposition of electric and magnetic dipoles and multipoles of the spheres. Since the permittivity of spheres is much larger than the host material, the electric and magnetic dipole fields are dominant. Thus, one set of spheres can offer electric dipole moments, and the other set can provide magnetic dipole moments. Because of the small-size spheres in terms of host wavelength, one can successfully assign the effective material parameters $(\varepsilon_{eff}, \mu_{eff})$ to the bulk composite. The constitutive parameters were formulated originally by Lewin in Ref. 10 considering the spheres resonate either in the first or second resonant modes of the Mie series. Then, Jylha *et al.* improved those formulations by taking into account the electric polarizabilities of spheres operating in the magnetic resonant modes.[11] In Ref. 11, HFSS software was also used to numerically model the periodic configuration where the perfect electric conductor (PEC) and perfect magnetic conductor (PMC) surfaces were located on the periodic sides of the structure. This method is applicable only if the electric and magnetic fields are polarized normal to the PEC and PMC surfaces, respectively. In a metamaterial, the electric and magnetic fields can, in general, be polarized in complex forms inside the unit cell and applying this technique may not be appropriate.

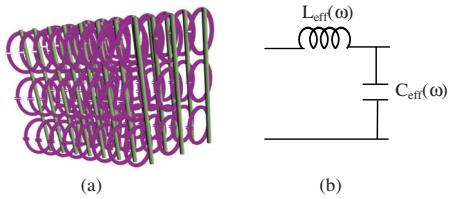

FIG. 1. (Color online) DNG metamaterial constructed from metallic loops and rods. (a) The geometry, and (b) its equivalent circuit model.

The advantages of only-dielectric metamaterial in comparison to its metallic counterpart are the better potential for fabrication from RF to optics, and the higher efficiency because of not having the metallic loss. In addition, one can achieve an isotropic metamaterial design utilizing spherical geometry inclusions. Further, the dielectric spheres offer wider bandwidth at the electric and magnetic eigenfrequencies due to the larger fraction of unit-cell volume that they can occupy.

It is worth noting that if the goal is to achieve a DNG medium at optical frequencies, one can use only one set of

spheres (magnetic resonant mode), and embed them inside a negative permittivity plasmonic host material, such as metals or semiconductors. This idea was first proposed by Seo *et al.* in Ref. 12. The obtained structure shows more robust characteristics over the double-spheres lattice design in terms of fabrication tolerance and bandwidth, although the loss of the host plasmonic medium (the metal) can be an issue.

The goal of the present work is to provide a comprehensive investigation of dielectric metamaterials. The physical insights and engineering concerns are addressed. We start with the periodic photonic band-gap (PBG) crystals, and demonstrate how the band-gap region is obtained as the result of periodicity along the propagation direction and diffraction phenomena between the unit cells. The near-field patterns before and after the gap region are plotted to better understand the PBG behavior. Then, we modify the geometry of the PBG crystal by considering finite size disks instead of the infinite rods. The performance is analyzed, and transmission coefficient and near-field patterns are determined. It is illustrated that the dielectric disks can interestingly create electric and magnetic dipole moments at their resonant modes, which can be successfully used for the metamaterial development. This process is basically nothing to do with the periodicity and unit-cell diffractions along the direction of propagation, and allows one to accomplish a metamaterial with very small-size ingredients. The concept is extended to spherical particles, and effective constitutive parameters $(\pm\varepsilon, \pm\mu)$ are presented. A DNG all-dielectric metamaterial is designed. The dielectric metamaterial is free of conduction loss and provides a relatively high efficiency. The periodic (or possible random) arrangement of particles also suppresses the radiation loss that each of the resonators produces individually. It is shown that by embedding the dielectric particles close to each other, the couplings between them are increased, and the bandwidth of a negative permittivity-negative permeability region is effectively enhanced. The complex metamaterial structures designed in this paper are modeled using an advanced and versatile in-house developed finite difference time domain (FDTD) technique.[13,14]

II. PERIODIC PHOTONIC CRYSTALS

Photonic crystals are a novel class of periodic dielectric structures that by offering engineered dispersion diagrams

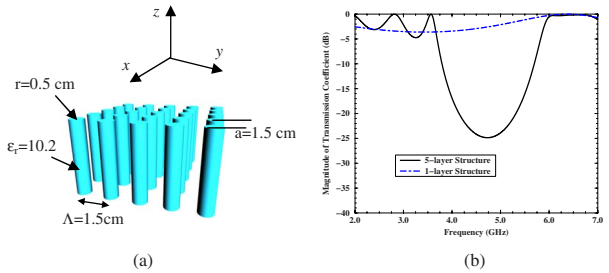

FIG. 2. (Color online) Periodic structure of dielectric rods. (a) The geometry, and (b) its transmission coefficient. Note that one layer of dielectric rods does not generate any band-gap region.

effectively manipulate the propagation of EM or optical waves.[15,16] The discovery of PBG crystals created unique opportunities for proposing novel devices in both microwave and terahertz frequencies.[17–19] The main benefit of PBG materials is their construction from all dielectric elements, which increases their feasibility for fabrication from RF to optics. Although in the beginning the focus was on the utilization of the stop-band region of PBG for controlling the waves, recently, other applications such as directive emission, negative refraction, superlensing, etc., with the use of other parts of the PBG dispersion diagram have been highlighted.[20,21] One fact that must be carefully considered is that the novel behaviors of the PBG are derived from the unit-cell interactions and periodic dielectric contrasts along the propagation direction, and one needs a specific unit-cell size to achieve the required diffractions for accomplishing the performance of interest. The problem is now twofold: first, the unit cell cannot be as small as one is interested in, and second, the diffraction phenomenon degrades the performance of the PBG in some specific applications such as directive emission or superlensing devices.

To show the effects of the unit-cell size and structure periodicity on the PBG performance, a periodic configuration of dielectric rods with a diameter of $d=1$ cm, permittivity of $\varepsilon_r=10.2$, and a lattice constant of $a=1.5$ cm is depicted in Fig. 2(a). The rods are infinite along the z direction, and periodic along the y direction. Five layers are considered in the x direction. The FDTD is applied to obtain the transmission coefficient for a plane wave with E_z-H_y polarization, propagating through the PBG structure (along the x direc-

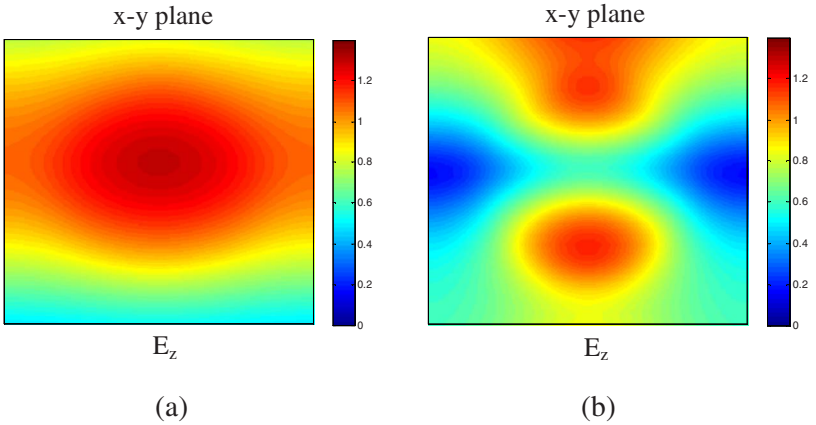

FIG. 3. (Color online) Near-field patterns for E_z in the x-y plane (one unit cell) for five-layer rods; (a) before band gap ($f_1=2.80$ GHz), and (b) after band gap ($f_2=6.60$ GHz). Note the confinement of dielectric and air modes inside the dielectric and air regions, respectively.

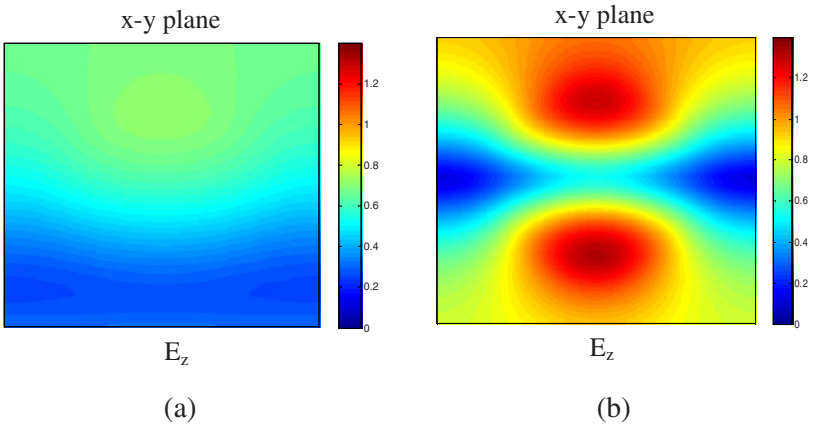

FIG. 4. (Color online) Near-field patterns for E_z in the x-y plane (one unit cell) for one-layer rods at (a) $f_1=2.80$ GHz, and (b) $f_2=6.60$ GHz.

tion). The result is plotted in Fig. 2(b). The periodicity of structure along the x direction opens up a stop-band region between the dielectric and air modes for $0.19<a/\lambda_0<0.29$ (−10 dB transmission level) for the electromagnetic (EM) wave. The size of the unit cell dominantly determines the frequency range of stop-band performance. The characteristic of the one-layer PBG (along the x) is also shown in Fig. 2(b). Because of the lack of periodicity and unit-cell diffractions, no band-gap region in the frequency of interest is observed.

The E_z near-field patterns of five-layer PBG before and after the band-gap region (at $f_1=2.80$ GHz and $f_2=6.60$ GHz) are shown in Fig. 3. It is observed that at frequencies before the band gap the electric field is concentrated inside the dielectric region, giving it a lower frequency, while the mode just above the gap has most of its power in the air region, so its frequency is raised a bit. This satisfies the electromagnetic variational theory applied to understand the PBG concept.[16] For the one-layer PBG near-field behaviors at f_1 and f_2 are obtained in Fig. 4, and one cannot observe the similar phenomena as what was obtained for the five-layer case.

Therefore, to achieve a desired performance utilizing the PBG concept (periodic dielectric contrast), having periodicity and a relatively large size unit cell are essential. One might be able to reduce the size of the unit cell by increasing the permittivity of the dielectric rod; however, this will increase the interactions between the unit cells causing more diffractions along the propagation direction, which might not be suitable for some applications. In the following sections, we will address how an engineered dispersion diagram may be successfully tailored using a different concept that is based on the creation of dipole modes inside the dielectric resonators. This will introduce a unique paradigm for the development of functional metamaterials.

III. DIELECTRIC DISKS: ELECTRIC AND MAGNETIC DIPOLE CREATION

In this section, we introduce the concept of electric and magnetic dipole moments, and address their potential applications for metamaterial realization. To begin, let us consider the five-layer PBG structure depicted in the previous section and modify the geometry by considering finite size disks with thickness $L=0.5$ cm. The geometry is shown in Fig. 5(a). The FDTD is applied to characterize the structure and obtain the transmission coefficient. The result is plotted in Fig. 5(b). No band-gap region is observed. Now, we increase the permittivity of dielectric disks to $\varepsilon_r=60$ such that a stop-band performance in the frequency range of $4.75<f(\mathrm{GHz})<5.10$ can be determined. Interesting enough, that even one layer of this design can also provide the band-gap phenomenon around the same center frequency ($f=4.94$ GHz), having of course a narrower bandwidth, as shown in Fig. 5(c).

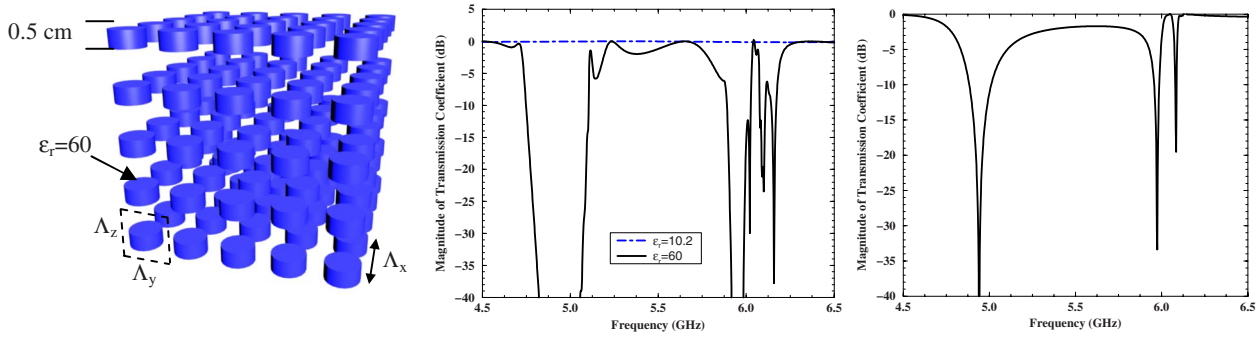

FIG. 5. (Color online) Array of all-dielectric disks. (a) The geometry ($\Lambda_x=\Lambda_y=\Lambda_z=1.5$ cm), and transmission coefficients for (b) five-layer structure, and (c) one-layer structure.

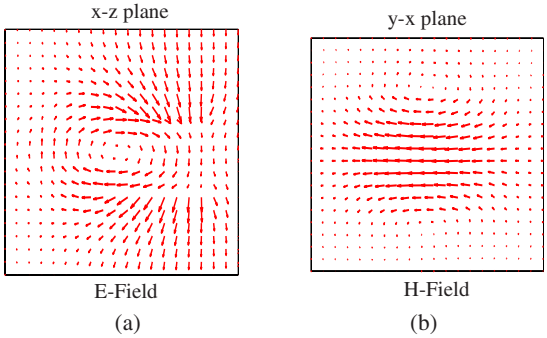

FIG. 6. (Color online) Field distributions inside one unit cell of the one-layer disks array at f_1=4.94 GHz ($HEM_{11\delta}$ mode). (a) E in the x-z plane, and (b) H in the y-x plane. Near fields are similar to those of a magnetic dipole oriented along the y direction.

To provide a physical understanding of this phenomenon, the electric and magnetic field patterns inside one unit cell of the one-layer disks array at f_1=4.94 GHz are plotted in Fig. 6 (snapshot in time). One can observe that the near-field patterns of the dielectric disk are very similar to those of a magnetic dipole oriented along the y direction. The near-field patterns at the second and third resonant frequencies f_2 =5.97 GHz and f_3=6.08 GHz are also plotted in Figs. 7 and 8, respectively. The disk at the second resonant frequency is almost equivalent to an electric dipole located along the z axis. The third mode has a resonant frequency very close to the second mode, and its magnetic field pattern in the equatorial plane exhibits an octupole characteristic, consisting of two linear quadrupoles rotated by 90° with respect to each other. Higher order resonant modes can also be generated by the dielectric disks utilizing the mutipole modes.

Because of the very large permittivity material of the dielectric disk, one can consider the structure as a resonator where most of the fields are localized inside the medium. Kejfez *et al.* have performed a comprehensive study of dielectric resonators in Ref. 22, and clearly illustrated the potential of dielectric cylindrical resonators for providing electric and magnetic dipole moments. Semouchkina *et al.* have also noticed the differences between the field patterns of infinite rods PBG and finite-size cylinders.[23] Peng *et al.* have

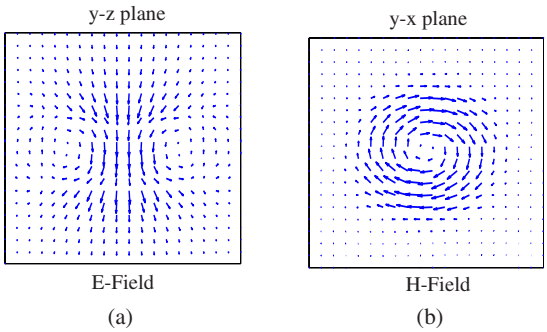

FIG. 7. (Color online) Field distributions inside one unit cell of the one-layer disks array at f_1=5.97 GHz ($TM_{01\delta}$ mode). (a) E in the y-z plane, and (b) H in the y-x plane. Near fields are similar to those of an electric dipole oriented along the z direction.

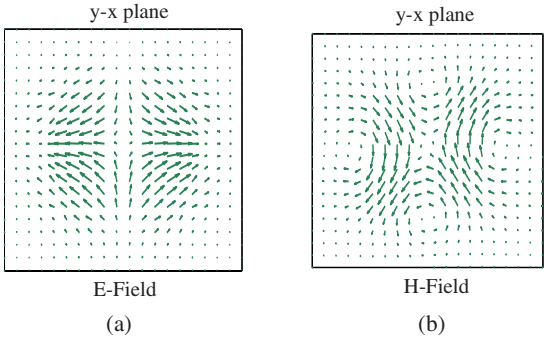

FIG. 8. (Color online) Field distributions inside one unit cell of the one-layer disks array at f_3=6.08 GHz ($HEM_{21\delta}$ octupole mode). (a) E and (b) H in the y-x plane.

also recently illustrated the electric and magnetic mode development inside the very high permittivity rods.[24] Considering the polarization of the plane wave excitation, the three resonant frequencies obtained in Fig. 5(c) can be attributed to $HEM_{11\delta}$, $TM_{01\delta}$, and $HEM_{21\delta}$ resonant modes, respectively.[22] The near-field patterns for an isolated finite-size cylinder for the above resonant modes have been plotted in Ref. 22, and they closely resemble what has been demonstrated here for the periodic array of the disks. Hence, the stop-band regions in Fig. 5(c) are derived from the resonant modes of the isolated disks, and thus even one layer of the structure can provide the band-gap property of interest.

The $HEM_{11\delta}$ mode is sometimes called *unconfined mode*, because in the limit, as $\varepsilon_r \to \infty$, its magnetic field does not vanished on the surfaces of the cavity resonator. This can be revealed from Fig. 6, where the magnetic field is normal to the magnetic wall boundary of the cavity and cannot be zero in the limiting case. In contrast, the $TM_{01\delta}$ mode is of the *confined* type, since its magnetic field is tangent to the boundary of the cavity, and in the limit, as $\varepsilon_r \to \infty$, it must be zero along the surface (see Fig. 7). The mode confinement behavior can also be readily seen by looking at the transmission coefficient plot in Fig. 5(c), where the $HEM_{11\delta}$ mode (magnetic dipole) presents a lower Q than the $TM_{01\delta}$ mode (electric dipole). The octupole performance of the $HEM_{21\delta}$ mode represents an inefficient radiator and consequently, its Q factor is very large. It is worth noting that although each of the disk resonators individually has some radiation loss, when we arrange them in the periodic fashion, the couplings between them are increased and the radiation loss is considerably suppressed.

Tailoring the dielectric disks allows one to successfully control the physical performance of the design. For example, as mentioned earlier, the resonant frequency of the $HEM_{21\delta}$ mode is very close to the electric dipole mode ($TM_{01\delta}$), and if the $TM_{01\delta}$ mode is the desired mode of operation, the $HEM_{21\delta}$ mode may create an undesirable nearby resonance effect, and one might be interested in suppressing it. This can be simply accomplished by placing a thin wire loop on the end face of the disk resonator where the electric field has a strong ϕ component, or, for instance, since the $TM_{01\delta}$ mode has a relatively strong electric field along the axis of rotation, it is possible to tune this mode by removing the cylindrical

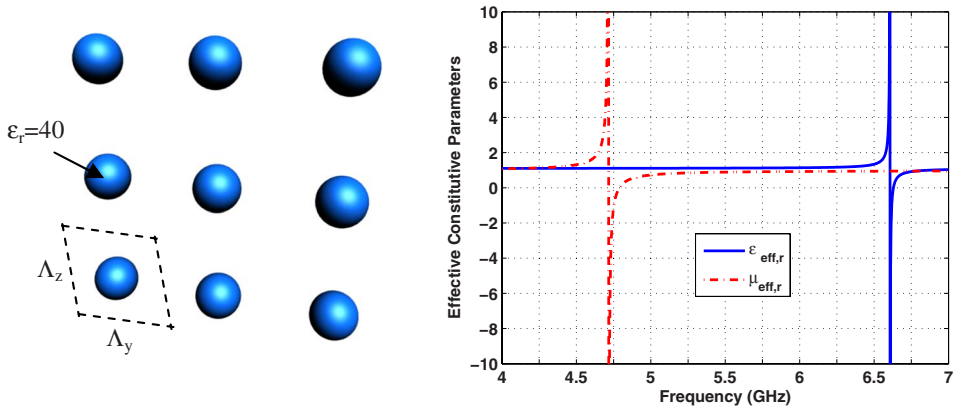

(a) (b)

FIG. 9. (Color online) Array of one-layer all-dielectric spheres. (a) The geometry ($\Lambda_y = \Lambda_z = 2.5$ cm), and (b) its effective constitutive parameters.

center section (leaving a doughnut shape) and replacing it by a movable dielectric rod.

In summary, the important conclusion of this section is the fact that dielectric resonators can successfully provide electric and magnetic dipole modes. The dipole moments can be considered as the alphabet for making metamaterials. For instance, using an array structure of the magnetic dipole disks (one layer) one can effectively provide a band-gap medium. The major advantage compared to the PBG concept is that the unit-cell interaction along the propagation directions is not required for achieving the functionality of interest. Basically, each of the disks itself provides the required resonant behavior. In general, by tailoring the electric and magnetic dipole moments in one unit cell one can make a building-block cell with the figure of merit of interest. Then, by making a material from these small-size cells, one can claim a metamaterial design with the homogeneous effective constitutive parameters $(\varepsilon_{eff}, \mu_{eff})$. This will be described in more detail in the next section.

IV. METAMATERIAL REALIZATION

The materials presented in the previous section are very helpful in providing a physical understanding of the dipole modes generation utilizing dielectric resonators. In this section, we apply this concept to design spherical particle-based metamaterials. Figure 9(a) shows a periodic array of dielectric spheres having high permittivity ε_p embedded inside the nonmagnetic host matrix ε_h. The structure has an isotropic unit cell. Using Mie theory, one can express the EM waves of each sphere as an infinite series of spherical vector functions $\mathbf{M}_n$ and $\mathbf{N}_n$. Applying the field transformation between the nonconcentric spheres, and using the boundary conditions, the array of spheres can be solved analytically.[10,25] It is assumed that the size of the spheres is comparable to their material wavelength, and small in terms of host material wavelength, so that the effective material parameters can be accurately defined for the structure. As demonstrated earlier, the dielectric resonators can offer electric and magnetic dipole moments, and higher order modes. Indeed, from the Mie series, it clears that the dominant modes $(n=1)$ are *TE* (magnetic dipole) and *TM* (electric dipole) waves. Around the eigenfrequencies of these modes one can assume the existence of only the electric and magnetic modes and obtain the effective material parameters $(\varepsilon_{eff}, \mu_{eff})$ for the periodic spheres as[8]

$$\varepsilon_{eff} = \varepsilon_h \left(1 + \frac{3\nu_f}{\dfrac{\varepsilon_p F(\theta) + 2\varepsilon_h}{\varepsilon_p F(\theta) - \varepsilon_h} - \nu_f} \right), \tag{1a}$$

$$\mu_{eff} = \mu_0 \left(1 + \frac{3\nu_f}{\dfrac{F(\theta) + 2}{F(\theta) - 1} - \nu_f} \right), \tag{1b}$$

where ν_f is volume fraction of the spheres, and function $F(\theta)$ is

$$F(\theta) = \frac{2(\sin\theta - \theta\cos\theta)}{(\theta^2 - 1)\sin\theta + \theta\cos\theta}, \tag{2}$$

with

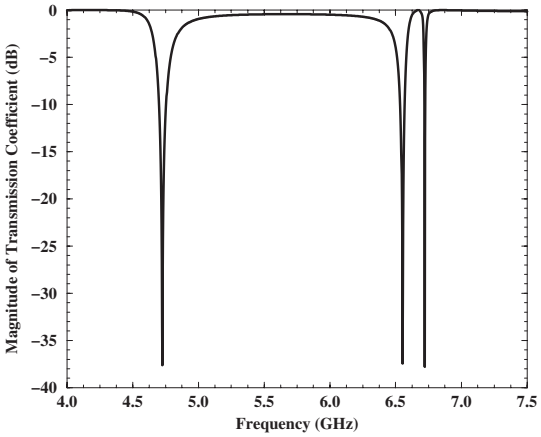

FIG. 10. Transmission coefficient for the all-dielectric spheres depicted in Fig. 9(a). The first and second resonances represent magnetic and electric resonant modes, respectively.

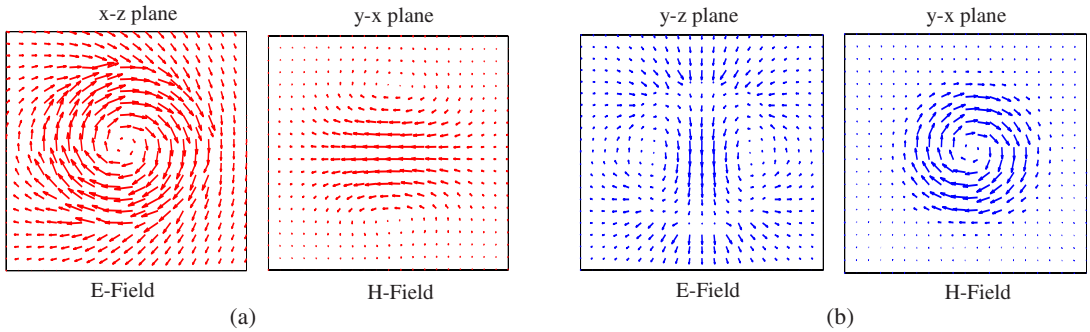

FIG. 11. (Color online) Field distributions inside one unit cell of the spheres array. (a) E in the x-z plane and H in the y-x plane at f_m=4.73 GHz, representing the magnetic dipole moment, and (b) E in the y-z plane and H in the y-x plane at f_e=6.55 GHz, representing the electric dipole moment. (1.5 cm×1.5 cm of the unit cell in the y-z directions is plotted).

$$\theta = k_0 r \sqrt{\varepsilon_{p,r}}, \tag{3}$$

where r is the radius of spheres. It is interesting to emphasize that the nonmagnetic spheres can create magnetism due to the magnetic dipole polarization.

The effective constitutive parameters of the periodic spheres depicted in Fig. 9(a), having dielectric constant $\varepsilon_{p,r}$ =40, radius r=0.5 cm, and unit-cell size Λ_x=1.5 cm, Λ_y =Λ_z=2.5 cm, are plotted in Fig. 9(b). The first resonant frequency at f_m=4.72 GHz is associated with the magnetic mode and the second resonance at f_e=6.61 GHz represents the electric mode. As described earlier, the magnetic mode is an unconfined mode and provides a wider bandwidth. This can be seen from Fig. 9(b) and Eq. (1), where one can find a larger bandwidth for the TE resonance in comparison to the TM resonance by a factor of about $\varepsilon_p/\varepsilon_h$. It is worth noting that above the resonant frequencies of magnetic and electric modes, negative permeability and negative permittivity materials are established, respectively. This will be used later in this section for the metamaterial realization of DNG behavior.

The FDTD is applied to characterize the structure and obtain the transmission coefficient for a plane wave propagating through the medium (one layer along x). The result is shown in Fig. 10. Comparing Fig. 9(b) with Fig. 10, one can observe that the analytical formulations (1) closely estimate the first two resonant frequencies determined through the FDTD full wave analysis (less than 1% error). However, as expected, the third resonant frequency at f=6.73 GHz cannot be predicted based on Eq. (1). In practice, the third resonant frequency can set an upper limit on the frequency band of the second mode where the effective permittivity is defined. It is interesting to note that the transmission coefficient behavior of the dielectric spheres is very similar to that of the dielectric disks [see Fig. 5(c)]. The near-field distributions are plotted in Fig. 11 for the first two resonant frequencies (f_m=4.73 GHz and f_e=6.55 GHz) and clearly validate the existence of magnetic and electric dipole polarizations.

Thus far, we have described how one can successfully realize a metamaterial with both electric and magnetic parameters utilizing only-dielectric resonators, fulfilling desired effective constitutive parameters. The next step is to investigate the possibility of increasing the bandwidth of the resonant modes. But, first let us clear one issue. Consider, for instance, the magnetic resonant mode of the one-layer periodic spheres [Fig. 9(a)], having −10 dB bandwidth of about BW=1.2%. It is well understood that each of the cavity resonators can be considered as a parallel LC circuit. Cascading the LC resonant circuits can increase the transmission coefficient bandwidth. In fact, increasing the number of layers

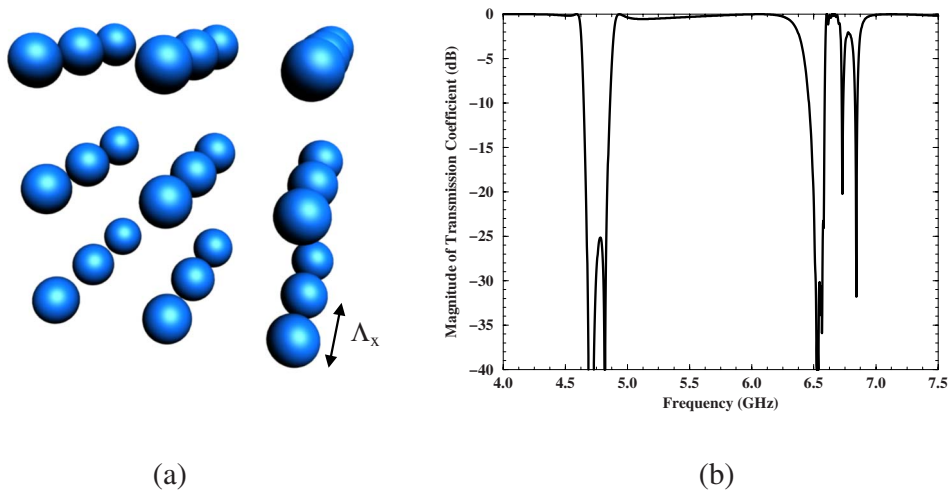

FIG. 12. (Color online) Array of three-layer dielectric spheres (Λ_x=1.5 cm). (a) The geometry, and (b) its transmission coefficient.

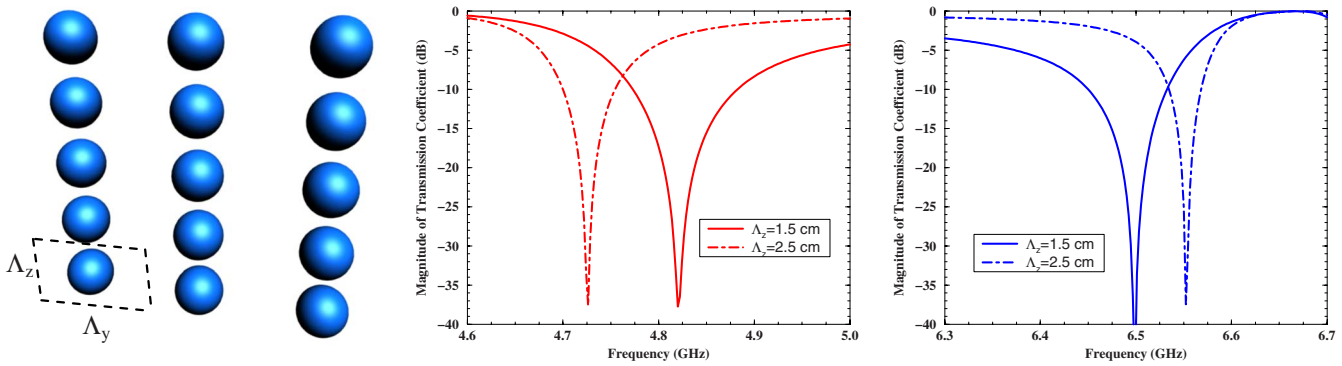

FIG. 13. (Color online) Bandwidth enhancement of metamaterial by increasing couplings between the elements (smaller unit-cell size), (a) the geometry, (b) transmission coefficient at the magnetic resonance, and (c) transmission coefficient at the electric resonance. The more the couplings the wider the bandwidth.

(parallel *LC* circuits) increases the transmission coefficient bandwidth. However, it should be noticed that this is nothing to do with the bandwidth of the metamaterial. The performance of three layers of the spheres designed in Fig. 9(a) is shown in Fig. 12. The transmission bandwidth is increased from 1.2% to about 4.6%; but, both one-layer and three-layer structures have almost the same μ_{eff} given by Eq. (1b), and of course the similar permeability bandwidth. Increasing the number of layers will simply increase the thickness of the structure.

In this work, a very unique approach for the bandwidth enhancement of metamaterials is presented. Recently, Mosallaei *et al.* demonstrated how the bandwidth of the negative permeability medium realized utilizing metallic embedded-loop circuits can be improved by increasing the couplings between the loop elements.[26] In fact, based on their circuit model analogy it is shown that the bandwidth of the negative permeability medium depends strongly on the coupling coefficient κ between the loops, and can be estimated from the following equation:

$$\frac{\Delta\omega}{\omega_p} = \frac{1}{\sqrt{1-\kappa^2}} - 1, \tag{4}$$

where ω_p is the resonant frequency of the loops, and $\kappa < 1$. The higher the coupling coefficient κ the larger the bandwidth. This concept is applied here to the all-dielectric metamaterial design. Basically, we increase the couplings between the spheres shown in Fig. 9(a), by bringing them closer to each other along the z direction, namely, assuming $\Lambda_z = 1.5$ cm [Fig. 13(a)]. Transmission coefficient for the magnetic mode is plotted in Fig. 13(b) illustrating a bandwidth enhancement of more than 100% compared to the original design ($\Lambda_z = 2.5$ cm). An almost similar observation for the electric mode resonance is illustrated in Fig. 13(c) (bandwidth is increased from 0.5% to 1.3%). Basically, when we make the spheres closer to each other, the mode radiation through the spheres is increased causing the reduction in the Q factor of each of the spheres, resulting in the bandwidth enhancement of the resonant modes. Slight shifts in

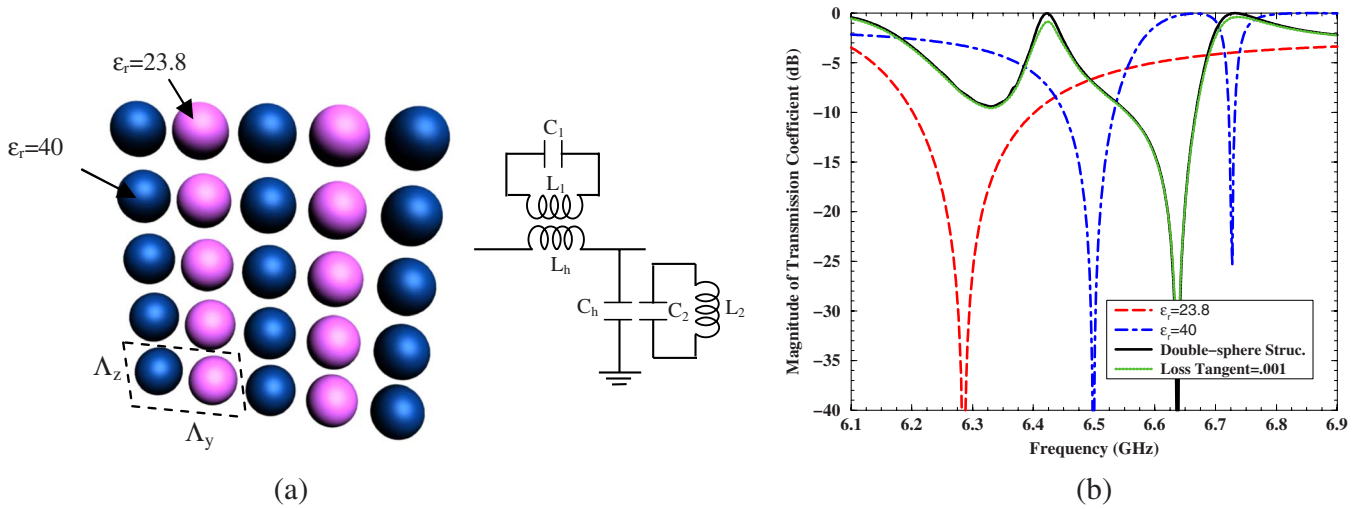

FIG. 14. (Color online) DNG metamaterial constructed from all-dielectric spheres, (a) the geometry ($\Lambda_y = 2.5$ cm, $\Lambda_z = 1.5$ cm), and its equivalent circuit model, and (b) transmission coefficient.

the resonant frequencies due to the coupling effects are also noted.

We will now investigate the development of double negative metamaterials using dielectric resonators. As highlighted earlier, and can be seen from Fig. 9(b), the periodic array of dielectric spheres can generate both negative effective permeability and permittivity, however, at different resonant frequencies (f_m=4.72 GHz, f_e=6.61 GHz). To obtain a DNG behavior around the same resonant frequency, a building-block unit cell constructed from two spheres having the same size but different dielectric constants $\varepsilon_{p1,r}$=40 and $\varepsilon_{p2,r}$=23.8, is optimized in Fig. 14(a). The set of spheres with $\varepsilon_{p1,r}$=40 creates negative effective permittivity about f_e=6.50 GHz, and the set of spheres with $\varepsilon_{p2,r}$=23.8 generates negative effective permeability about f_m=6.29 GHz. Figure 14(b) presents transmission coefficients of both sets, where stop-band regions are determined in the negative material frequency ranges. It must be mentioned that in the constructed lattice of both spheres [Fig. 14(a)], the electric mode has a higher Q compared to the magnetic mode, and hence, the coupling effect of the sphere with dielectric $\varepsilon_{p2,r}$=23.8 on the electric resonance should be larger than that of the sphere with dielectric $\varepsilon_{p1,r}$=40 on the magnetic resonance. This phenomenon is carefully explained from another point of view in Ref. 11; as is discussed the electric polarizability of the dielectric sphere operating in the magnetic resonance has an influence on the electric mode sphere, causing the electric resonance of the double-sphere lattice to be slightly lower than that of the single-sphere lattice (less than 1% shift). The magnetic resonance stays almost the same (non-magnetic spheres). Thus, in Fig. 14(b), the electric resonance of the single-sphere lattice should be slightly shifted down to envision the negative permittivity region of the double-sphere lattice. Considering this, a region with both negative ε and μ is accomplished. Transmission coefficient for the double-sphere unit cell is shown in Fig. 14(b), demonstrating an almost total transmission in the DNG region, around f=6.42 GHz. The phase of the field distribution at f=6.42 GHz inside one layer of the metamaterial is shown in Fig. 15. The positive slope for the phase in the central region of the layer clears the establishment of the DNG medium

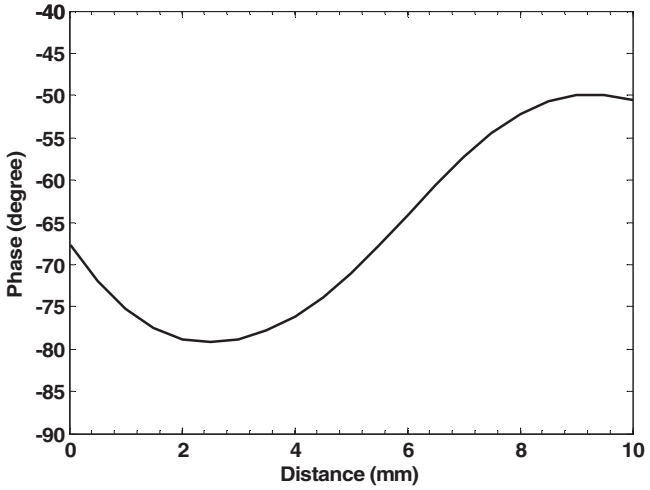

FIG. 15. Phase distribution of the electric field E_z inside the layer of DNG metamaterial [Fig. 14(a)] at f=6.42 GHz. The plane wave propagates from left to the right where the phase is increased in this direction. The positive slope for the phase in the central part of the layer is a demonstration of the backward wave generation.

(backward wave). The electric and magnetic field intensities inside the unit cell at this frequency are also shown in Fig. 16. One can clearly observe the development of electric and magnetic dipole modes that provide the required effective material parameters. This also validates the existence of the dipolar modes assumption, made in the derivation of Eq. (1). The effect of the loss is also studied, by considering spheres with a dielectric loss tangent of tan δ=0.001. The result is plotted in Fig. 14(b), illustrating less than −1 dB transmission loss in the DNG region. Utilizing dielectric materials with better loss tangents can of course provide a higher efficiency.

The same concept can be used to design a DNG metamaterial realized utilizing dielectric disks, which might be easier for fabrication in some cases. The geometry is depicted in Fig. 17(a). Transmission coefficients and field patterns at f=5.97 GHz are evaluated in Figs. 17(b) and 18. Similar observations as the spherical particles are accomplished.

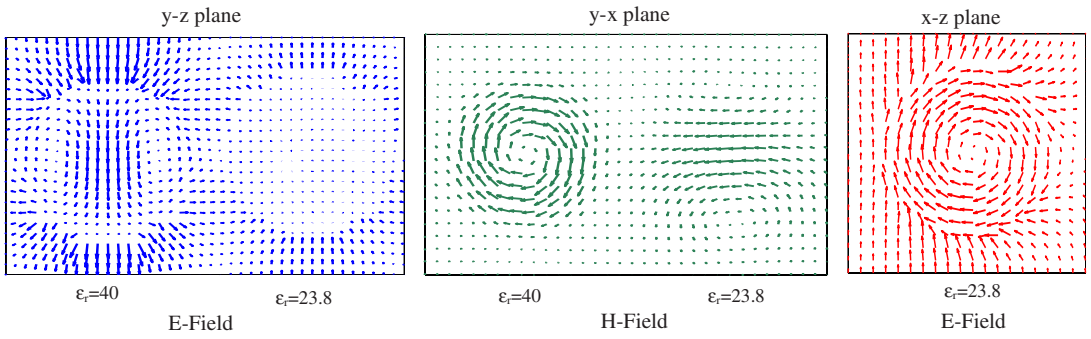

FIG. 16. (Color online) Field distributions inside one unit cell of the DNG metamaterial [Fig. 14(a)] at f=6.42 GHz. (a) E in the y-z plane, (b) H in the y-x plane, and (c) E in the x-z plane. Note the creation of electric and magnetic dipole moments inside the unit cell of the spheres of ε_r=40 and ε_r=23.8.

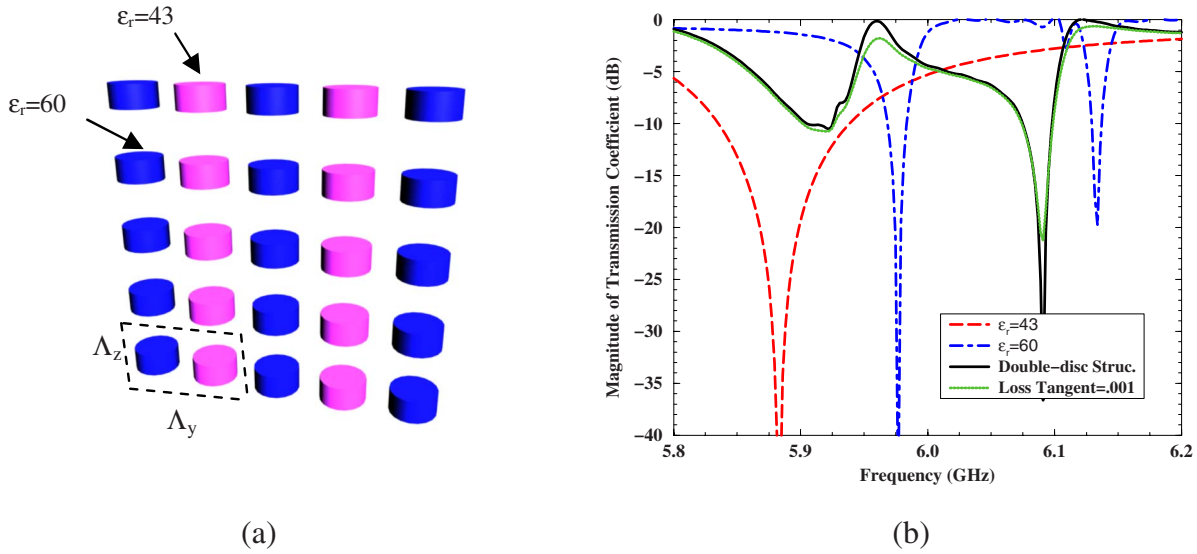

FIG. 17. (Color online) DNG metamaterial constructed from all-dielectric disks, (a) the geometry (Λ_y=2.5 cm, Λ_z=1.5 cm), and (b) its transmission coefficient.

V. OPTICAL METAMATERIALS

Realization of metamaterials at terahertz frequencies is also of great interest due to the possibility of designing novel nanoscale devices in the infrared and visible regimes.[27–32] The concept of all-dielectric metamaterials can be extended to the optical frequencies; however, because of the fabrication limitations one needs to use smaller value dielectric materials for the resonating inclusions. In this case, larger-size resonators may be implemented. Figure 19(a) depicts an array of gallium phosphide (GaP) spheres with permittivity 12.25 and a dielectric loss tangent of tan δ=0.001. The diameter of spheres is 170 nm. Transmission coefficient performance is shown in Fig. 19(b), where the development of magnetic and electric resonant modes can be observed. One must notice that because of the low dielectric material of the spheres and their relatively large physical size the couplings between the resonators are increased. This will generate some difficulty in tuning the DNG medium if two sets of spheres are used. Although the existing coupling may not be desirable from the fact that the electric and magnetic resonances are coupled, it can be beneficial from the point that one can successfully tailor a backward wave using the strong interaction between the spheres. Work is currently under progress in this direction.

Alternative approaches will be to embed one set of dielectric spheres inside a plasmonic host medium as obtained by Seo *et al.*;[12] or to use Drude material coated spheres as proposed by Wheeler.[32] Here, we investigate the former method by characterizing the performance of the periodic array of GaP spheres implanted inside cesium (Cs) host material with a measured plasma wavelength λ_p=0.41 μm and a damping constant γ of 51×10^{12},[12] shown in Fig. 20(a). Note that if one operates close to the plasma frequency, the index of host material is small, and physically large-size spheres are still electrically small in comparison to the host wavelength. Transmission coefficient of the composite structure is shown in Fig. 20(b). The spheres operate at their magnetic resonant mode and can provide negative effective permeability [see Fig. 19(b)]. A combination of this with the negative permit-

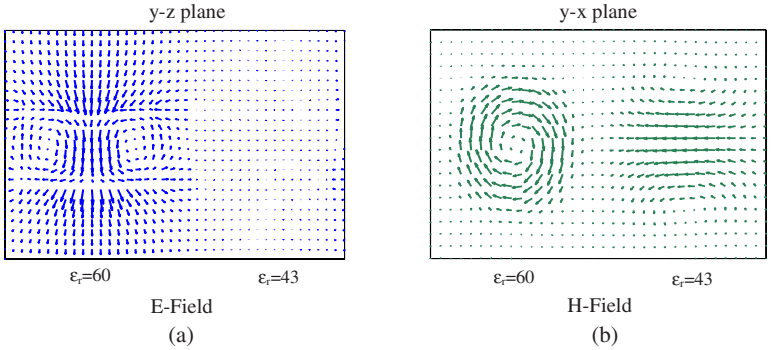

FIG. 18. (Color online) Field distributions inside one unit cell of the DNG metamaterial [Fig. 17(a)] at f=5.97 GHz. (a) E in the y-z plane, and (b) H in the y-x plane. Note the creation of electric and magnetic dipole moments inside the unit cell of the disks of ε_r=60 and ε_r=43.

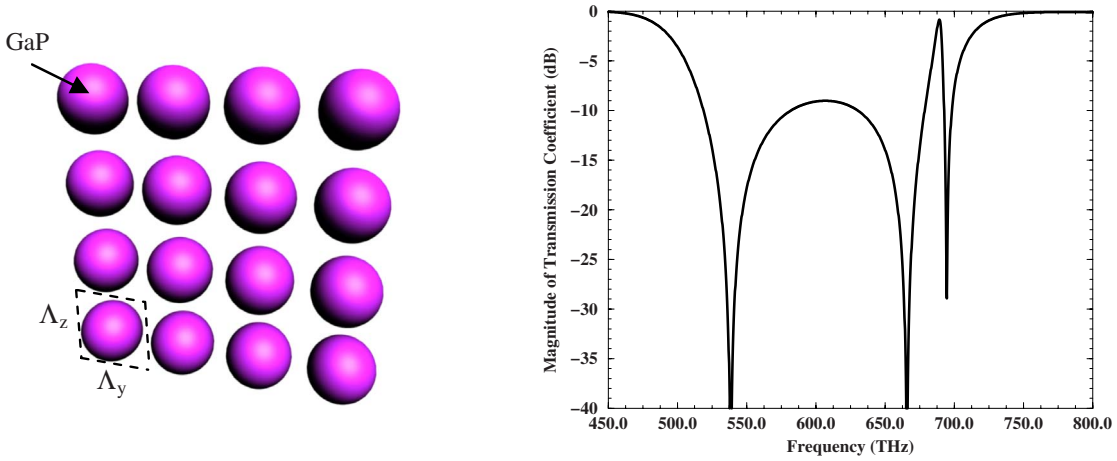

FIG. 19. (Color online) Metamaterial nanostructured spheres. (a) The geometry ($\Lambda_y=\Lambda_z=250$ nm), and (b) its transmission coefficient. Note the generation of magnetic and electric resonances.

tivity of cesium below its plasma resonance offers DNG behavior. In comparison to the double-sphere resonators design, here only one set of resonators is involved and a wider bandwidth can be expected. In addition, the spheres operate in their magnetic mode frequency range, which inherently offers a lower Q than the electric mode. Transmission loss for this case is about −1.1 dB. The magnetic field pattern at $f=529$ THz is shown in Fig. 20(c).

VI. SUMMARY

In this paper, a comprehensive investigation of all-dielectric metamaterials is addressed. The FDTD full wave analysis is applied to characterize the interactions of EM-optical waves with the periodic array of metamaterials, and tailor required designs. Electric and magnetic near-field patterns are established to highlight the physical insights.

Photonic crystals are searched first, and it is described that the band-gap phenomenon appears as a result of the periodic dielectric contrasts along the propagation direction. Then, the concept of electric and magnetic dipole modes generation for metamaterial development is presented. Dielectric disk and spherical particle resonators are implemented to create required dipole moments. Arrangements of electric and magnetic dipole moments in one unit cell tailor the metamaterial to the application of interest. The beauty of the developed metamaterial is that even one unit cell of the structure can provide the figure of merit of interest, and the interactions between the cells is not essential, as was the case for the PBG. This will allow for making the small-size unit cell, and defining the effective constitutive parameters accurately. Further, a random arrangement might have the potential of offering the similar desired properties, especially in the spherical resonator case where the unit cell is isotropic.

The physics of electric and magnetic dipole moments are explored. It is shown that the magnetic resonance is an unconfined mode and has a lower Q than the confined electric

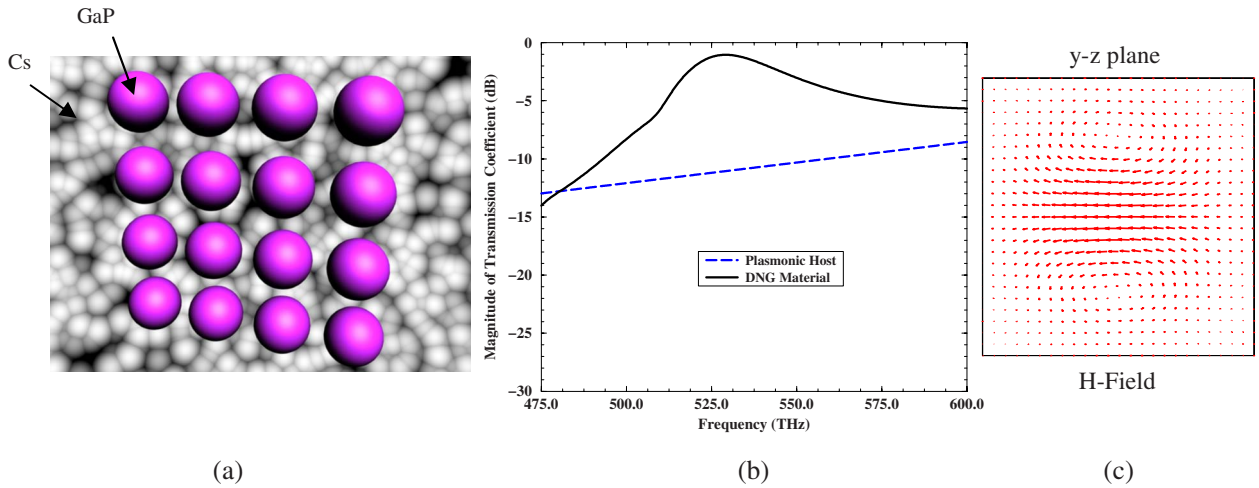

FIG. 20. (Color online) DNG optical metamaterial constructed from nanostructured dielectric spheres (operating in magnetic mode) embedded in negative permittivity host. (a) The geometry, (b) transmission coefficient, and (c) H field in the y-z plane at $f=529$ THz.

resonant mode. A unique approach is proposed to increase the bandwidth of the resonant particles. Basically, by bringing the dielectric resonators closer to each other, the radiation couplings between them are increased, resulting in lowering the Q of each of the resonators. This will establish bandwidth enhancement. Dielectric metamaterials are free of conduction loss and can provide high efficiency performance.

A DNG metamaterial constructed from two sets of spheres, having the same size but different materials, is developed. One set of spheres provides negative permittivity, and the other set offers negative permeability, accomplishing the double negative metamaterial. One can also design a double-sphere lattice DNG metamaterial using the spheres of different sizes but having the same materials. Development of negative index media at terahertz frequencies using plasmonic materials is also studied.

In general, all-dielectric metamaterials appear very promising for addressing some of the important physical and engineering concerns, such as the loss and bandwidth. They are quite feasible for fabrication in both microwave and IR-visible spectrums.

ACKNOWLEDGMENT

This work is supported in part by the U.S. Air Force Office of Scientific Research (AFOSR) Grant No. FA9550-07-1-0133.

*hosseinm@ece.neu.edu

[1] J. B. Pendry, Phys. Rev. Lett. **85**, 3966 (2000).
[2] R. A. Shelby, D. R. Smith, and S. Schultz, Science **292**, 77 (2001).
[3] N. Engheta and R. W. Ziolkowski, *Metamaterials: Physics and Engineering Explorations* (John Wiley & Sons, Inc., New York, 2006).
[4] C. Caloz and T. Itoh, *Electromagnetic Metamaterials: Transmission Line Theory and Microwave Applications* (John Wiley & Sons, Inc., New York, 2006).
[5] G. V. Eleftheriades and K. G. Balmain, *Negative-Refraction Metamaterials* (John Wiley & Sons, Inc., New York, 2005).
[6] J. B. Pendry, A. J. Holden, D. J. Robbins, and W. J. Stewart, IEEE Trans. Microwave Theory Tech. **47**, 2075 (1999).
[7] J. B. Pendry, A. J. Holden, D. J. Robbins, and W. J. Stewart, J. Phys.: Condens. Matter **10**, 4785 (1998).
[8] C. L. Holloway, E. F. Kuester, J. Baker-Jarvis, and P. Kabos, IEEE Trans. Antennas Propag. **51**, 2596 (2003).
[9] O. G. Vendik, and M. S. Gashinova, in Proceedings of the 34th European Microwave Conference, Amsterdam, Netherlands, 2004, pp. 1209–1212.
[10] L. Lewin, Proc. Inst. Electr. Eng. **94**, 65 (1947).
[11] L. Jylha, I. Kolmakov, S. Maslovski, and S. Tretyakov, J. Appl. Phys. **99**, 043102 (2006).
[12] B. J. Seo, T. Ueda, T. Itoh, and H. Fetterman, Appl. Phys. Lett. **88**, 161122 (2006).
[13] H. Mosallaei and Y. Rahmat-Samii, Electromag. J. **23**, 135 (2003).
[14] A. Taflove and S. C. Hagness, *Computational Electrodynamics: The Finite-Difference Time-Domain Method*, 3rd ed. (Artech House, MA, 2005).
[15] E. Yablonovitch, Phys. Rev. Lett. **58**, 2059 (1987).
[16] J. D. Joannopoulos, R. D. Meade, and J. N. Winn, *Photonic Crystals* (Princeton University Press, Princeton, NJ, 1995).
[17] IEEE Trans. Microwave Theory Tech. **47** (1999).
[18] E. Burstein and C. Weisbuchin, in *Confined Electrons and Photons: New Physics and Applications*, Proceedings of NATO Advanced Study Institute of Confined Electrons and Photons: New Physics and Applications, Italy, July 13–26, 1993; *Confined Electrons and Photons: New Physics and Applications* see also in Series B: Physics (Plenum, New York, 1995), Vol. 340.
[19] *Photonic Band Gap Materials*, edited by C. M. Soukoulis, Proceedings of NATO Advanced Study Institute Photonic Band Gap Materials, Elounda, Crete, Greece, June 18–30, 1995; *Photonic Band Gap Materials*, edited by C. M. Soukoulis see also Series E Applied Sciences (Kluwer Academic, Dordrecht, Germany, 1966), Vol. 315.
[20] S. Enoch, G. Tayeb, and B. Gralak, IEEE Trans. Antennas Propag. **51**, 2659 (2003).
[21] P. V. Parimi, W. T. Lu, P. Vodo, and S. Sridhar, Nature (London) **426**, 404 (2003).
[22] D. Kajfez and P. Guilllon, *Dielectric Resonators* (Artech House, Inc., Dedham, MA, 1986).
[23] E. A. Semouchkina, G. B. Semouchkin, M. Lanagan, and C. A. Randall, IEEE Trans. Microwave Theory Tech. **53**, 1477 (2005).
[24] L. Peng, L. Ran, H. Chen, H. Zhang, J. A. Kong, and T. M. Grzegorczyk, Phys. Rev. Lett. **98**, 157403 (2007).
[25] P. C. Waterman and N. E. Pedersen, J. Appl. Phys. **59**, 2609 (1986).
[26] H. Mosallaei and K. Sarabandi, IEEE Trans. Antennas Propag. **55**, 45 (2007).
[27] N. Engheta, A. Salandrino, and A. Alù, Phys. Rev. Lett. **95**, 095504 (2005).
[28] A. Alu and N. Engheta, J. Opt. Soc. Am. B **23**, 571 (2006).
[29] A. K. Iyer and G. V. Eleftheriades, J. Opt. Soc. Am. B **23**, 553 (2006).
[30] V. M. Shalaev, W. Cai, U. K. Chettiar, H. K. Yuan, A. K. Sarychev, V. P. Drachev, and A. V. Kildishev, Opt. Lett. **30**, 3356 (2005).
[31] D. Korobkin, Y. Urzhumov, and G. Shvets, J. Opt. Soc. Am. B **23**, 468 (2006).
[32] M. S. Wheeler, J. S. Aitchison, and M. Mojahedi, Phys. Rev. B **73**, 045105 (2006).